OPEN

Quantum Mechanical Metric for Internal Cohesion in Cement Crystals

C. C. Dharmawardhana[1], A. Misra[2] & Wai-Yim Ching[1]

[1]Department of Physics and Astronomy, University of Missouri – Kansas City, 5110 Rockhill Road, Kansas City, MO 64110, USA, [2]Department of Civil, Environmental, and Architectural Engineering, University of Kansas, 1530 W 15th Street, Lawrence, KS 66045, USA.

Calcium silicate hydrate (CSH) is the main binding phase of Portland cement, the single most important structural material in use worldwide. Due to the complex structure and chemistry of CSH at various length scales, the focus has progressively turned towards its atomic level comprehension. We study electronic structure and bonding of a large subset of the known CSH minerals. Our results reveal a wide range of contributions from each type of bonding, especially hydrogen bonding, which should enable critical analysis of spectroscopic measurements and construction of realistic C-S-H models. We find the total bond order density (TBOD) as the ideal overall metric for assessing crystal cohesion of these complex materials and should replace conventional measures such as Ca:Si ratio. A rarely known orthorhombic phase Suolunite is found to have higher cohesion (TBOD) in comparison to Jennite and Tobermorite, which are considered the backbone of hydrated Portland cement.

E lectronic structure and inter-atomic bonding characteristics are central to the comprehensive understanding of the atomic-scale structure and properties of calcium silicate hydrates (CSH) that are synthesized as Portland cement hydration products. The emerging interest in atomic structure-property relationships is due to the increasingly significant environmental, social and economic impact of the global Portland cement usage and production, which currently stands at 2 billion metric tons. Current experimental findings based upon a variety of spectroscopic and high-resolution microscopic techniques suggest a poorly crystalline or completely disordered atomic structure of these hydrates in hardened cement paste[1]. Based on these experimental data, a number of structural models have been proposed, either as binary solutions[2–4] or through theoretical modeling using Jennite and Tobermorite type crystals as starting structures[1,5–8]. These efforts have resulted in a wide range of models for C-S-H[9–12] that are either based on solution theory or limited atomistic simulations using classical molecular dynamics (MD). A key missing ingredient in these efforts is the understanding of bonding characteristics of both the crystalline CSH as well as the more disordered C-S-H. For brevity and clarity, we will follow the cement chemistry notation of CSH and CS to represent calcium silicate hydrate and anhydrate crystals, respectively, and C-S-H to exemplify the more general structure of calcium silicate hydrate found in hardened cement paste.

Crystalline CSH phases range from almost amorphous to highly ordered crystalline phases. Due to their varying degree of crystallinity and the difficulties associated with isolation of pure phases, many uncertainties remain about the composition and structure even for CSH phases of high crystallinity. Furthermore, due to the complexity of CSH structures, quantitative bonding information, especially H-bonding (HB), are not accessible purely by experimental means without the aid of robust atomistic model for proper interpretation, giving rise to the proverbial chicken-egg problem. In the light of this critical gap in knowledge, it is of paramount importance to investigate a wide variety of crystalline CSH phases with well-documented crystal structures. Such studies will provide an in-depth insight on the variations in bonding characteristics in relation to the composition and structures of these materials. Without this information, the atomistic models of C-S-H proposed[13] in the literature will remain speculative.

The uncertainty with respect to position of "H" was discussed previously in a study of four crystalline CSH crystals[14]. Since HB has a significant presence in CSH, it plays a crucial role in the behavior of these materials. This fact has been generally recognized but rarely studied quantitatively. Clearly, even for crystalline phases, the bonding information cannot be determined purely from experimental data in the absence of refined structures of these phases. Here we take a materials genomic approach and theoretically investigate a broad range of CSH crystals using accurate first principles methods. Out of the 30 crystalline phases listed by Richardson in the 2008 review article[1], we choose 15 CSH crystals with well-documented structural information, their four possible

anhydrous precursors, and portlandite. We begin with fully optimized atomic structures of these crystalline phases. We use a supercell approach to address the issue of partial occupancy at certain sites in some crystals. The electronic structures of the refined structures are then calculated. Subsequently, we quantitatively evaluate the bonding characteristics of these crystals through bond order (overlap population) calculations. We analyze the results following the modified Strunz classification of minerals according to the degree of polymerization of the silicate chains in these crystals. The data obtained from crystalline phases can help in the interpretation of experimental spectroscopic measurements leading to realistic models that are consistent with the both electronic-scale and atomistic-scale behaviors for the C-S-H phase in hardened Portland cement.

Classifications of CSH crystals. A comprehensive review by Richardson *et. al.*[1] includes an extensive list of 30 CSH crystal phases that are categorized into six groups following Taylor et al.[5]. However, the CSH crystals can be more appropriately classified according to the Strunz classification[15] by considering the silica chain polymerization. The notion of silica chain polymerization also has implications on the products of the complex hydration process[16,17] and carbonation or biological degradation[18,19] that occurs in Portland cement paste. It has been speculated that the maturation of cement paste involves increasing polymerization of primarily isolated Si tetrahedra to dimers, trimmers and pentamers, eventually forming a 3-dimensional silicate framework[20].

Table 1 lists 20 crystal phases with well-documented atomic positions used in this study placed into four groups: *a*, Clinker and hydroxide phase; *b*, nesosubsilicates; *c*, sorosilicates; and *d*, ionosilicates. Each group in Table 1 is arranged in ascending order of calcium to silicon (C/S) ratio. The clinker phases (a.1 and a.2) and the Portlandite (a.3) are placed in **group a**. Portlandite is included in this group since it forms the basis for hydration of cement. The remaining crystals are grouped according to the Strunz scheme. In this scheme, the silicate units at each polymerization step are indicated by Q^n, where the Si tetrahedron is connected to **n** other silicate tetrahedra.

For example, an isolated silicate tetrahedron not connected to any other is denoted by Q^0. The nesosubsilicates with isolated $[SiO_4]^{-4}$ groups are placed in **group b**. These CSH phases possess the lowest degree of polymerization. The sorosilicates with $[Si_2O_7]^{-6}$ groups in the next polymerization step are placed under **group c**. For these phases, the $[Si_2O_7]^{-6}$ is connected to two isolated tetrahedra via one bridging-O to form the so-called pyrogroups. Thus, all silicon tetrahedra are Q^1. These silicon tetrahedra are linked via non-bridging O, to six-, seven- or even eight fold-coordinated Ca atoms. A special case of sorosilicate structures are those with mixtures of isolated tetrahedra (Q^0) and finite triple chains (Q^2), in which the silicon tetrahedra are connected to 6 and 8-fold coordinated Ca atoms. The **group d** contains the inosilicates. These comprise structures with infinitely long chains with a wide variety of C/S ratios, ranging from 0.50 in Nekoite (d.1) to 1.5 in Jennite (d.8). According to the degree of polymerization, the phases in this group could be subdivided into inosilicates with single chains (all tetrahedra are Q^2), and double chains (2/3 Q^2 and 1/3 Q^3). The representative crystals from each group are illustrated in Figure 1. They are Alite (a.2) for **group a**; Afwillite (b.1) for group **b**; Suolunite (c.2), Kilichoanite (c.3) for **group c**; and Anomalous T11 A (d.2), forshgite (d.7) for **group d**. Similar images of all 20 crystals are displayed in the supporting information (SI) as Figure S1.

Electronic structures of CSH. Although the atomic structures of the crystals in Table 1 are generally available[21], inaccuracies exits along with some missing data. Section 1 in SI and Figure S1 give additional information on the fully relaxed and corrected structures to reconcile with the chemical formula where applicable. Table 1 gives a summary of the crystal symmetry, chemical formulas, theoretical density, C/S ratio and calculated electronic band gap. Out of the 20 crystals studied, 4 are anhydrate phases; 2 contain purely isolated water molecules, 5 include both isolated water and hydroxyl groups, and rest have only hydroxyl groups. In CSH, hydroxyl groups are mostly connected to Si (Si-OH) but in some instances (b.1, b.2, b.3, c.2, c.4, c.5, d.6 and d.7) they can be connected to Ca (Ca-OH) as well. The

Table 1 | Mineral names, crystal symmetry and space group symmetry, chemical formulas, Calculated C/S, density, and band gap (in eV) of the 20 crystals in this study

	Mineral Name	sy:sg	Chemical formula	Ca/Si	ρ (g/cc)	E_g
(a). Clinker/Hydroxide phases						
a.1	Belite	O: $P\ 1\ 21/n\ 1$	$2(CaO)\ SiO_2$	2.00	3.316	4.65
a.2	Alite	M:P-1	$3(CaO)\ SiO_2$	3.00	3.084	3.68
a.3	Portlandite	M: $P\ -3\ m\ 1$	$Ca(OH)_2$	Inf	2.668	3.50
(b). Nesosubsilicates						
b.1	Afwillite	M:P1	$Ca_3(SiO_3OH)_2 \cdot 2H_2O$	1.50	2.590	4.26
b.2	α-C2SH	O: $P\ 2_1/b\ 2_1/c\ 2_1/a$	$Ca_2(HSiO_4)(OH)$	2.00	2.693	4.37
b.3	Dellaite	Tc:P-1	$Ca_6(Si_2O_7)(SiO_4)(OH)_2$	2.00	2.929	4.12
b.4	Ca Chondrodite	M: $P\ 1\ 1\ 2_1/b$	$Ca_5[SiO_4]_2(OH)_2$	2.50	2.828	4.24
(c). Sorosilicates						
c.1	Rosenhahnite	Tc:P-1	$Ca_3Si_3O_8(OH)_2$	1.00	2.874	4.49
c.2	Suolunite	O: $F\ d\ 2\ d$	$Ca_2[Si_2O_5(OH)_2]H_2O$	1.00	2.649	4.87
c.3	Kilchoanite	O: $I\ 2\ c\ m$	$Ca_6(SiO_4)(Si_3O_{10})$	1.50	2.937	4.40
c.4	Killalaite	M: $P\ 1\ 2_1/m\ 1$	$Ca_{6.4}(H_{0.6}Si_2O_7)_2(OH)_2$	1.60	2.838	3.85
c.5	Jaffeite	Tg: $P\ 3$	$Ca_6[Si_2O_7](OH)_6$	3.00	2.595	3.92
(d). Inosilicates						
d.1	Nekoite	Tc: P1	$Ca_3Si_6O_{15} \cdot 7H_2O$	0.50	2.204	4.29
d.2	T11 Å	M: $B\ 1\ 1\ m$	$Ca_4Si_6O_{15}(OH)_2 \cdot 5H_2O$	0.67	2.396	4.15
d.3	T14Å	M: $B\ 1\ 1\ b$	$Ca_5Si_6O_{16}(OH)_2 \cdot 7H_2O$	0.83	2.187	4.04
d.4	T 9 Å	Tc: C1	$Ca_5Si_6O_{17}\ 5H_2O$	0.83	2.579	4.57
d.5	Wollastonite	Tc: P-1	$Ca_3Si_3O_9$	1.00	2.899	4.62
d.6	Xonotlite	Tc: A-1	$Ca_6Si_6O_{17}(OH)_2$	1.00	2.655	4.27
d.7	Foshagite	Tc: P-1	$Ca_4(Si_3O_9)(OH)_2$	1.33	2.713	4.41
d.8	Jennite	Tc:P-1	$Ca_9Si_6O_{18}(OH)_6 \cdot 8H_2O$	1.50	2.310	4.43

Sy = crystal symmetry.
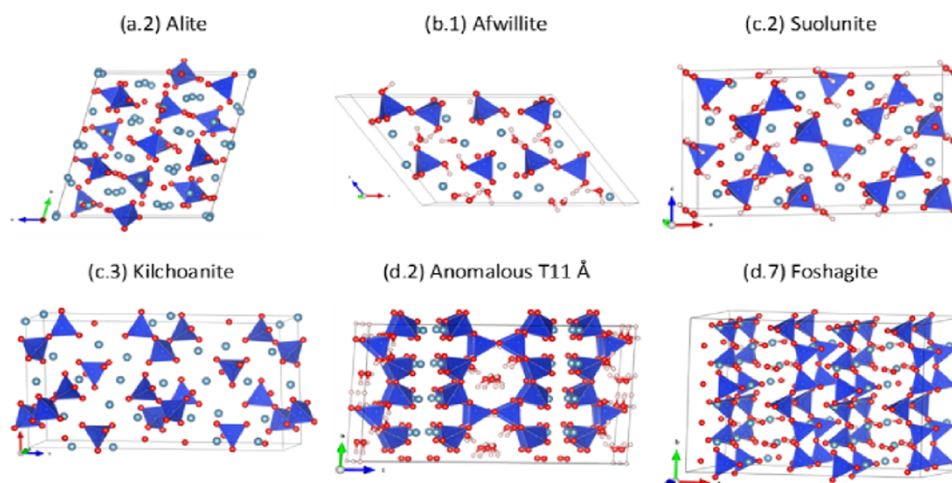Sg = space group symmetry.

Figure 1 | Ball-stick figures of representative crystals to illustrate the structures of each group of CSH and CS crystals: (a.2) Alite; (b.1) Afwillite; (c.2) Suolunite; (c.3) Kilchoanite; (d.2) Anomalous T11 Å; (d.7) Foshagite.

calculated band structures for the 20 crystals are displayed in Figure S2. The zero of the energy is set at the highest occupied state, or the top of the valence band (VB). As expected, all crystals have large band gaps ranging from 3.50 eV to 4.87 eV and exhibit flat top of VB except a.3. The bottom of the conduction bands (CB) of all crystals have large curvatures suggesting small electron effective mass. Analysis of the partial density of states (PDOS), indicates that the lower part of the VB is from O-2s orbitals and the upper part is from O-2p orbitals of the non-water O whereas the lower CB originates mostly from Ca-3d orbitals. There is a significant contribution from Si-3d orbitals to the upper part of the VB as well. High quality band structure based on accurately relaxed structure is important in assessing the electronic structure because experimentally measured structures are usually not sufficiently accurate. This is particularly true for hydrated crystals with water molecules. Discrepancy with the experimentally assigned "H" positions was pointed out in earlier work[14]. Table 2 show the VASP relaxed crystal parameters and the percent deviation from the experimentally reported values. The experimental crystal parameters are given in the SI Table S1. The relaxed crystal parameters in general vary 1–2% compared to the reported experimental values but in some cases such as b.1 and b.4, they can be as high as −4.1%. The highest deviation is in the

angle γ of the awfillite (b.1) crystal structure. This is a highly hydrated phase and we find considerable deviation in the hydrogen positions from the reported structure. This is explained in more detail in bottom of page 6. These deviations are larger than those usually found in other inorganic crystals. Obviously, there are large uncertainties in the data reported by different groups using different methods measured at different times for some of these CSH crystals. Hence, accurate theoretical computations based on density functional theory can provides the much needed consistency for CSH crystal structures based upon which reliable properties can be evaluated.

Bond order calculation in CSH. The bond order (BO) between each pair of atoms represents the quantitative measure of the bond stiffness and strength[22]. They are important in revealing the origin of internal cohesion in the CSH crystals. We obtain the BO values between every pair of atoms in the crystal using the first-principles orthogonalized linear combination of atomic orbitals (OLCAO) method[23] (see Method Section and Supplementary Information for details). Figure 2 shows the BO vs bond length (BL) distributions for four representative CSH crystals from each group (a: alite, b: afwillite, c: suolunite, and d: jennite). Different bond types in each crystals

Table 2	The crystal parameters (% error from experimentally reported values)					
	a(Å)	b(Å)	c(Å)	α°	β°	γ°
a.1	5.565(-1.1)	6.8(-0.6)	9.363(-0.4)	90(0)	94.70(-0.6)	90(0)
a.2	11.733(-0.8)	14.298(-0.9)	13.743(-0.7)	104.80(0.2)	94.36(0.3)	90.11(0)
a.3	3.614(-0.6)	3.614(-0.6)	4.958(-1.1)	90.18(-0.2)	89.82(0.2)	120.025(0)
b.1	16.57(-1.5)	5.719(-1.4)	11.764(-0.7)	87.59(2.8)	127.06(-0.5)	93.65(-4.1)
b.2	9.535(-0.5)	9.228(-0.5)	10.777(-1)	90(0)	90(0)	90(0)
b.3	6.888(-0.5)	7.028(-1.1)	12.952(-0.4)	90.10(0.7)	97.29(0)	98.28(0)
b.4	8.956(-0.4)	11.556(-0.9)	5.111(-0.7)	90.56(-0.6)	89.28(0.8)	108.71(-0.4)
c.1	7.052(-1.4)	9.548(-0.7)	6.883(-1)	108.78(-0.1)	95.73(-0.9)	95.34(0.6)
c.2	19.988(-1.1)	6.036(-0.8)	11.239(-1.1)	90(0)	90(0)	90(0)
c.3	11.527(-0.9)	5.13(-0.8)	22.204(-1.2)	90(0)	90(0)	90(0)
c.4	20.638(-0.8)	15.607(-0.9)	6.898(-0.9)	90(0)	97.17(0.5)	89.87(0.1)
c.5	10.085(-0.5)	10.084(-0.5)	7.538(-0.5)	90 (0)	90(0)	120(0)
d.1	7.665(-1)	9.797(0)	7.418(-1.1)	110.94(0.7)	103.59(-0.1)	86.69(-0.2)
d.2	6.736(0)	7.451(-0.9)	22.73(-1.1)	89.63(0.4)	90.42(-0.5)	122.22(0.8)
d.3	6.706(0.4)	7.416(0.1)	28.589(-2.1)	90.70(-0.8)	92.45(-2.7)	122.65(0.5)
d.4	11.414(-1.2)	7.416(-1)	11.48(-0.1)	98.36(0.8)	97.05(0.1)	90.23(-0.2)
d.5	8.009(-0.9)	7.381(-0.8)	7.139(-1)	90.08(-0.1)	95.53(-0.2)	103.44(0)
d.6	8.786(-0.8)	7.422(-0.8)	14.193(-1.2)	89.95(0)	90.66(-0.3)	102.25(-0.1)
d.7	10.423(-1)	7.367(-0.1)	7.159(-1.7)	90.07(-0.1)	106.48(-0.1)	89.98(0)
d.8	10.732(-1.5)	7.349(-1.2)	10.784(1.3)	103.22(-1.9)	94.78(2.3)	110.24(-0.5)

(Ca-O, Si-O, H-O-H, -(O-H), $H_2O\cdots H_2O$ and $-(O\cdots H)$)) are as indicated. As evident, there are two types of OH bonds. The strong covalently bonded ones and the weaker HBs. Further, there are two types of covalent O-H bonds: those within the water molecules (H-O-H) which do not contribute to internal cohesion, and those in the hydroxyl ions -(O-H), which attach to silicates (Si-OH) or Ca ions (Ca-OH). The HBs also have two categories: HBs between water molecules ($H_2O\cdots H_2O$, shown as inset of Figure 2 for b.1), and all other types of HBs that are not exclusively between two isolated water molecules. For example, the HBs, such as $Si-(O\cdots H)O-Si$ and $H_2(O\cdots H)O-Si$, that are particularly significant are shown as inset of Figure 2 for c.2 and d.8, respectively. As an overall measure of the crystal cohesion, we define the total BO (TBO) to be the sum of individual BO values and the total bond order density (TBOD) as the TBO normalized by the crystal volume.

The pie charts in Figure 2 give the percentage contribution from different types of bonds to the TBO. (Note: We have ignored the BO contribution from covalent O-H bonds from water molecule in calculating the percentage contributions since they do not directly contribute to the overall cohesion.) Figure 2 gives an overall representative picture of the distribution and relative strengths of different bond species in CSH crystals. The broad, almost continuous distribution of Si-O BO values within a fairly narrow range of Si-O BL clearly indicates that the bond stiffness/strength, not the bond length is the primary reason as to why the spectral features associated with Si-O bond often appear as broad peaks[24]. It is also remarkable that HBs cover a wide range of BO and BL in these materials and have a significant contribution to the TBO. The effects of HBs have been widely speculated in experimental spectroscopic techniques but never clearly explained. In the following, we describe the BO distributions for crystals in each group in relation to their structural characterization, showing the complex picture of different BO contributions to the crystal cohesion.

Bond order distribution for each group. Figure S3 displays the plots of BO versus BL and the percentage contribution from different types of bonds to the TBO for all 20 crystals. In **group a**, Belite (a.1) and Alite (a.2), contain only Q^0 silicates. The Si-O bonds have a narrow BO distribution centered at $\sim$0.27 with BL centered at $\sim$1.65 Å. The much weaker Ca-O bonds exhibit a larger BO and BL dispersion ranging from 0.02 to 0.10 and 2.25 Å to 3.50 Å, respectively. The Ca-O bonds in Belite have almost evenly spread BO and BL, while those in Alite show some clustering between 2.27 Å to 2.55 Å. These BO and BL distributions clearly explain why the strong and
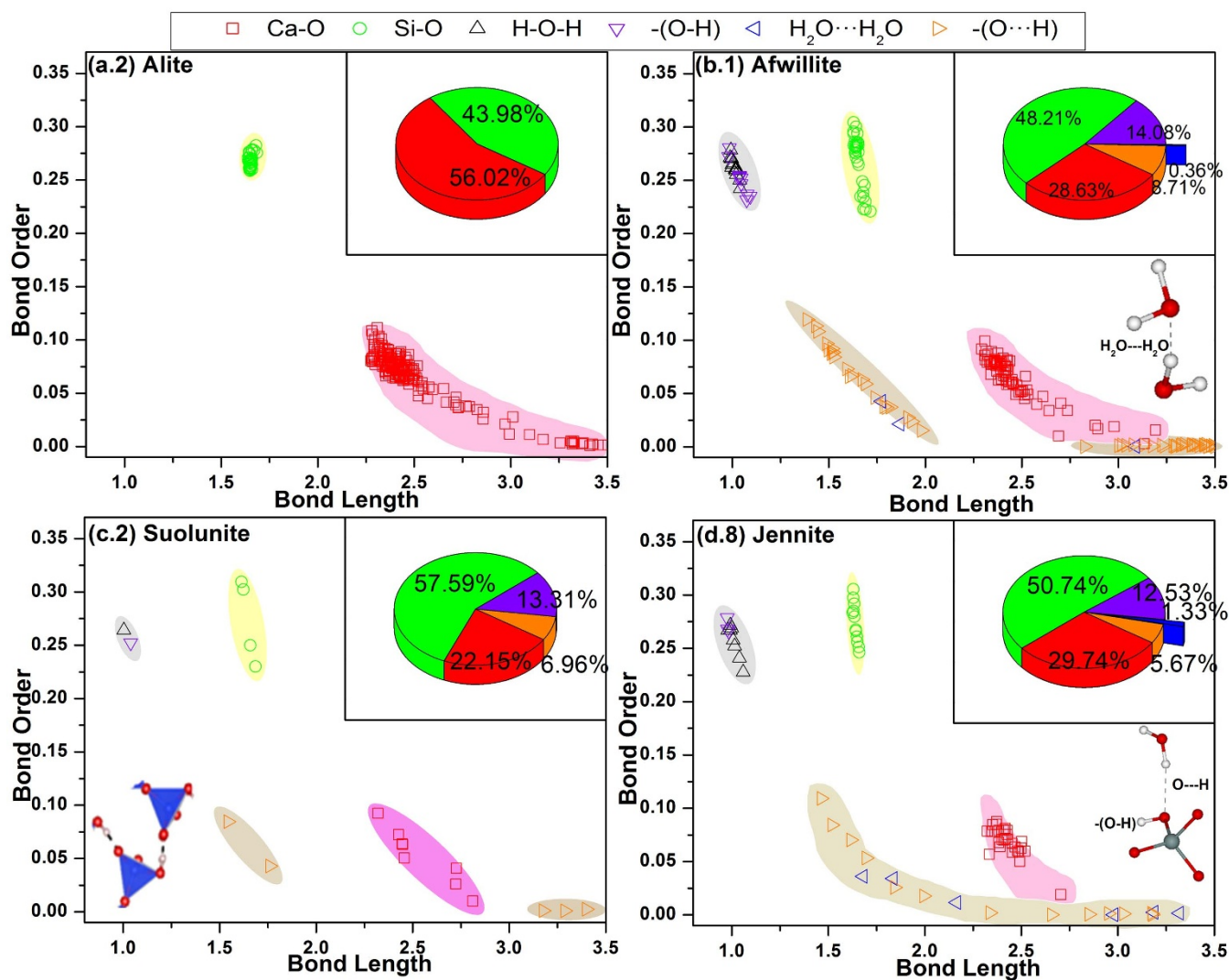

Figure 2 | Distribution of bond order vs. bond length in four representative crystals. (a.2) Allite; (b.1) Alwillite; (c.2) Suolunite; and (d.8) Jennite. Symbols for different types of bonds are shown at the top, ''-'' for covalent bond, ''…'' for hydrogen bond. The pie chart in the inset shows the percentage of different types of bonding: red, Ca-O; green, Si-O; violet covalent –(O-H); orange, other HB; blue, HB between H2O. Lower insets show different types of hydrogen bonds.

considerably sharper Si-O peaks dominate the experimental vibrational spectroscopic analyses of these minerals in contrast to the broad and weaker peaks associated with Ca-O bonds[25,26]. It is noteworthy that in Portlandite (a.3) the BO for Ca-O bonds (0.223 with a BL of 2.381 Å) is much stronger than the Ca-O bonds in the above CS crystals and all other CSH crystals.

The **group b** crystals contain the Q^0 silicates as well as covalent O-H bonds and HBs. In this group, only Afwillite contains water molecules. These crystals have a broadly dispersed Si-O BO although with well-defined narrowly ranged BL. The lower Si-O BO is generally associated with the Si-OH (hydroxyl) bond, while the higher BO with Si-O bonds within the tetrahedral unit. The Ca-O BO in **group b** crystals is significantly smaller and shows a narrow distribution over a wide range of BL. Further, the covalent O-H bonds and HBs exhibit a wide range of BO and BL as expected. For all the crystals in this group, the contributions from Ca-O, O-H bonds and HBs to the TBO are almost 50% or more. For example, in Afwillite (b1), the contributions to the TBO are as follows: Si-O (48.2%), Ca-O (28.6%), O-H (14.1%) and O···H (8.7%). Here the covalent O-H bonds are connected to the silicate tetrahedral units $[HSiO_4]^{-3}$ through HBs whose BLs varies between 1.38–1.98 Å with significant BO values. Therefore, the -O···H contribution in Afwillite is the highest (8.71%) in this group. Rastsvetaeva et al.[24], in their IR spectrum analyses of Afwillite[27], have assigned the characteristic vibrational modes of the so-called zundel cation $(H_2\text{-}O\cdots H\cdots OH_2)^+$, or $(H_5O_2^+)$[28]. However, in our BO analysis, we do not observe this zundel cation structure. Instead, we find two HBs connecting water molecules with close proximity on either side of CaO layer (parallel to b-c plane) as shown in Figure 1 (b.1). Clearly, the interpretation of the IR spectrum could have immensely benefitted from the relaxed structure and BO calculations. In contrast, for α-C2SH (b.2), which contains both Si-OH and Ca-OH, the HB related to Si-OH is relatively stronger (BO = 0.066) compared to those linked to Ca-OH (BO = 0.014). The stronger HBs in α-C2SH (b.2) can be attributed to the fact that this crystal is formed under the high temperature hydrothermal conditions and is stable up to very high temperature[20]. The other two crystals in **group b**, Dellaite (b.3) and Ca-Chondrodite (b.4), show negligible contribution from the HBs because of the larger O···H separations. The Si-O bond, the Ca-O bond and the covalent O-H bond make primary contribution to TBO in these two crystals.

Crystals in the **group c** have an even wider distribution of Si-O BO values than **group b**, ranging from 0.18 to 0.35. The contribution from Si-O bonds to TBO is generall, larger than in **group b** whereas contribution from HBs is comparatively less. In this group, Kilchoanite (c.3) is a naturally occurring anhydrous crystal[29] with two types of silicate chains (Q^0 and Q^2) coexisting[30]. For crystals other than Kilchoanite (c.3), the O-H covalent bonds are clustered in a very narrow range similar to **group a and b** and the HBs follow the similar range as in **group b** (1.5 Å–1.80 Å). Although the **group c** crystals share the Strunz classification, they exhibit wide differences in structural and bonding characteristics. For example, the Killalaite (c.4) is a complex non-stoichiometric crystal with partial occupancy. It is composed of Q^1 silicate chains via a corner sharing O with the Si-O-Si angle of 124.8°. This crystal contains both Si-OH and Ca-OH units. The Si-O BO distribution is very broad (0.195–0.322) over a relatively narrow range in BL (1.60–1.72 Å). The HBs have relatively high BOs (0.045–0.102) with a BL in the range of (1.50–1.74 Å). The highest BO of HBs are Si-OH···O and Ca-OH···O. The percentage contribution to TBO from Si-O, Ca-O, O-H, and HBs are 54.3%, 34.33%, 10.03% and 1.33% respectively. On the other hand, Jaffeite (c.5) has a completely different structure and bonding with 12 covalent OH bonds in the form of Ca-OH but virtually no HBs. All the hydroxyl groups connected to Ca are directed away from the disilicate chains. Clearly, Jaffeite (c.5) is an outlier in terms of BO contributions compared to the other crystals in **c**. It has the lowest Si-O

contribution (34.1%) among the 20 crystals considered, hence the lowest TBOD. Of all the crystals in **group c**, Suolunite (c.2) is the most conspicuous. It contains primarily Q^1 Si-tetrahedra, as opposed to others that have both Q^0 and Q^2. Suolunite (c.2) is the only crystal in this group that contains water molecules, and is the only naturally occurring CSH crystal to have a $CaO:SiO_2:H_2O$ ratio of $1:1:1$[31]. All water molecules in Suolunite (c.2) have a consistent covalent bond length of 1.0033 Å. Since these water molecules are far apart so the $H_2O\cdots H$ HBs are absent. All the other HBs have short BL (1.5–1.76 Å) and relatively strong BO (0.042–0.084). Both Q^0 and Q^1 type silicates units in Suolunite (c.2) have one covalent O-H bond which also make HBs with the nearby O of the silicate chain with a BL (1.543 Å) and BO (0.085). The rest of HBs are from water molecule to the O of the adjacent silicate chains. It is interesting to note that –O···H has twice as large BO value than the HBs from water molecules. Suolunite (c.2) and Rosenhahnite (c.1) have same C/S ratio but the latter has no water molecules. Hence, the HBs contributions to the TBO are significantly small. We will return to more focused discussion on Suolunite later.

In **group d** crystals, the contribution of Si-O bonds in the infinite silicate chain structures dominates the TBO. However, the Si-O contribution to the TBO generally decreases as the C/S ratio increases. In addition, the layer separation, H_2O/OH content and crystal symmetry also affect the BO contributions. The CSH crystals in this group are amongst the most hydrated, except Wollastonite (d.5) which is an anhydrous precursor phase with 71.8% Si-O bonds and 28.2% Ca-O bonds[32]. The Si-O BO values of this group exhibit dispersion primarily due to small distortions from the ideal tetrahedral unit and the hydroxyl ions connecting the silicate chains and Ca. Two types of silicate chains are observed: (1) the single silicate chain as those found in d.1, d.3, d.4, d.5, d.7 and d.8; and (2) the double silicate chain in which 2 silicate chains from either side of the interlayer are connected via a bridging-O as in d.2 and d.6[20]. The presence of silicate chains leads to a layered structure of these minerals as well as high contribution of Si-O to the TBO. The interlayer separations between layers range from 4.95 Å in Foshagite (d.7) to 14 Å in T14 (d.3). The layered structure formed by these chains has a significant effect on the mechanical anisotropy of these crystals. Typically, water molecules and Ca reside in interlayer cavities and govern the interlayer cohesion[14]. For example in Nekoite (d.1), the interlayer (of separation 7.6Å) contains all Ca and H_2O. In this case, the Ca-O bond contributes 15.24% and the HBs contribute 5.21% to the interlayer cohesion. In contrast, the T11 (d.2) has H_2O in the interlayer but no Ca, thus HBs contribute 4.04%, whereas in T14 (d.3) and T9 (d.4), which has both Ca and H_2O, the Ca-O bond contributes 4.07% and 4.86% and the HBs contribute 5.48% and 3.17%, respectively to the to the interlayer cohesion. The difference in T14 (d.3) and T9 (d.4) is attributed to the lack of double silicate chains in former and the presence in later. Further, Xonotlite (d.6) and Foshagite (d.7) have unusually low contribution of HBs since these crystals contain only hydroxyl ions. In **group d**, Jennite (d.8), which has been widely considered as part of the C-S-H phase in hydrated cement, has the highest contribution of HBs (6.99%) to the interlayer cohesion.

Discussion and conclusion

We have presented the calculated electronic structure of 15 CSH crystals, 4 anhydrous precursor crystals and portlandite crystal. Band structures show all crystals are large band gap insulators. The BO topology and their contribution to the overall cohesion via TBO are analyzed. We found no specific rule common to all crystals but observed some trends for each group separately. The BO, TBO and TBOD of the various crystals clearly shows (1) the diverse degree of contributions of the various bond types to the overall crystal cohesion, (2) the variety of HBs, (3) the BO dispersion within each bond types in CSH, and (4) the importance of accurate crystal structure whose volume determines the TBOD. The traditional criterion for

classifying CSH crystals using C/S ratio is rather rudimentary in view of these diversities. We propose the total bond order density (TBOD) as an accurate quantum mechanical metric to classify the CSH crystals that provides far deeper insight to cohesion and strength of these materials.

Figure 3(a) shows the plot of TBOD vs the C/S ratio showing an approximate inverse relationship. It is apparent that crystals with the same C/S ratio can have very different TBOD. Since TBOD is more sensitive to the bonding and relevant to cohesion, its use for classifying CSH crystals is most appropriate. This plot also shows that the four groups discussed above do not cluster together in relation to the TBOD. **Group *c*** has a wide range of C/S as well as TBOD. However, **group *d***, believed to be closest to hydrated cement, has a narrow distribution in C/S but a wider TBOD range. Roughly speaking, we can divide the 20 crystals into to 3 groups according to their TBOD – high, medium and low. Crystals a.1, b.4 and c.5 belong to the low TBOD group mainly because of the high C/S ratio. On the opposite end, b.1 from **group *b***, c.1 and c.2 from **group *c*** and d.1, d2 and d4 from **group *d*** belong to the high TBOD group. The rest of 10 crystals belong to the medium TBOD group which mostly from **group *d*** crystals. The mixing of groups based upon Strunz classification and a weak correlation of TBOD with C/S ratio signifies the complex interplay and tradeoffs between the covalent bonds and HBs in these CSH structures. Although, Q^n chains in **group *d*** crystals tend to reduce C/S ratio, interlayer hydroxyl, water and HBs drastically alter the TBOD by increasing the effective volume without modification to C/S ratio. For example, crystal T14 (d.3) has a low C/S ratio but still has medium TBOD. The reason is that there are two types of silicate. Both d.2 and d.4 structures have double silicate chains whereas d.3 has only single silicate chains, which affects the TBOD considerably.

Measured mechanical properties for CSH crystals are difficult to obtain due to various practical limitations such as challenges in synthesizing single crystals, fast reaction with atmospheric water etc. Thus, there are only a few of CSH/CS phases where the mechanical properties were obtained experimentally. For example, the clinker phases Belite (a.1) and Alite (a.2), which have well-defined stoichiometric structures, are reported to have experimentally measured Young's modulus (E) between 140–130 GPa and 147–135 GPa respectively[33,34]. Similar experiments reported the E for Portlandite (a.3) to be in the range 36–48 GPa[34–38] depending on the porosity and a bulk modulus value of 39.65 GPa[39]. The bulk modulus of the crystal Toberomite 14Å (d.3) obtained recently using high pressure synchrotron X-ray diffraction to be 47 GPa[40] Using these limited experimental values, we find that the average of the measured E values for a.1, a.2 and a.3 crystals increase as a function of TBOD and show a near linear fit. In addition, the measured bulk modulus found for the two crystals, i.e. a.3 and d.3 also increase with TBOD. At this stage it is premature to correlate experimental mechanical properties with calculated TBOD. We intend to study this further with the calculated mechanical properties to find possible trends of mechanical properties with the TBOD.

Since Ca, Si and H are the primary components of the various bond types in CSH, it is useful to examine the complex interactions amongst the bond types by investigating the TBOD as function of Ca : Si : H ratio. Figure 3(b) shows the color-coded ternary plot of TBOD map with respect to Ca : Si : H composition. The resultant contour plot gives a vivid illustration of the possible locations for phases with high TBOD which appear to concentrate in the region where Ca : Si : H = 0.25 : 0.25 : 0.5. We note that Soulunite (c.2) with C/S ratio equal to 1 has the highest TBOD out of the 20 crystals investigated and according to our criterion, would be closest to the ideal composition and structure. The electronic structure and bonding of Soulunite has not been investigated until now. In the SI, we have further discussed its electronic structure with the presentation of its total density of states (DOS) and partial density of states (PDOS) resolved in accordance with the atoms involved in different

types of bonding. The narrow green and yellow areas in Figure 3(b) represent the medium TBOD. The wider blue regions represent the low TBOD regions.

In C-S-H (cement hydrates), it is known that infinite chain structures are absent[1]. On the other hand, it is widely believed that mixtures of tobermorite (d.2-d.4) and jennite (d.8) form the template or backbone of the C-S-H disordered structure. However, the TBOD and the BO calculations show that C-S-H structures in hydrated cements cannot simply be surmised as mixtures of CSH crystals or even some disordered form of these mixtures. In this regard, the following three aspects become clear: (1) the significant contribution of HBs and their role in affecting the BO of each bond type, (2) the significant dispersion in BO of the strong Si-O bonds with small BL variation, and (3) the variation in the BO of relatively weaker Ca-O bond. Since the interplay between different components from the structures cannot be explicitly quantified by known experiments[7], detailed electronic structure and bonding information are necessary to interpret experimental findings, especially in spectroscopic studies such as in Raman, IR and NMR measurements[18,24,41]. The implication is that attempts to use vibrational spectroscopy, such as IR or Raman, for structural interpretation have to be viewed carefully with special attention paid to small features and nuances, such as peak width and asymmetry.

From the viewpoint of mechanical properties, which are highly important for this material class, we note that silicates with strong covalent bonds are expected to contribute significantly to the overall crystal stiffness under small deformation. However, hydrated crystals with a low degree of polymerization may have considerable contributions to the materials stiffness via HBs in the HB network. Bond order analysis on crystals with finite silicate chains shows that H_2O, OH and HB network all play a key role in the cohesion of crystals. More significantly, the Si-O covalent bonds are unlikely to be the main source of crystal strength as often reported in the literature[42]. In multi-component crystals that include ionic, covalent and hydrogen bonds, the nonlinearity of mechanical response, the failure and the fracture behavior is often controlled by the weaker ionic or hydrogen bonds. Indeed, in these complex material systems, different atomic-scale deformation mechanisms trigger and persist under different loading paths[43]. For the CSH crystals as well as the more disordered C-S-H, both the silicate polymerization and the BO of various bond types will affect the deformation mechanisms. In this respect, highly polymerized structures, such as Tobermorite and Jennite, are likely to have highly anisotropic mechanical response with stiff response along the silicate chains complimented by planes of weaknesses. Suolunite, which has the highest TBOD, a high contribution of HBs and a low degree of polymerization of silicates, is likely to have a comparably high stiffness and absence of weak planes.

In conclusion, we have presented a compelling argument for using a quantum mechanical metric, the BO and the TBOD as the most important criterion to assess the crystalline cohesion in CSH crystals. This metric encompasses effects of both the geometric factors and the interatomic interactions. Therefore, the BO and TBOD provide a much more in depth measure for the overall behavior of this diverse class of materials. The TBOD should certainly replace the long-standing and traditionally used C/S ratio in classifying cement materials. Of the 15 CSH crystals studied, the inconspicuous crystal Suolunite turns out to have the highest TBOD, and the ideal composition, structure and bonding characteristics for cement hydrate. This finding should serve as an impetus for cement scientists engaged in molecular scale engineering of hydraulic cements. Synthesis of new anhydrous precursors or hydration pathways that lead to Suolunite type hydration products could yield robust infrastructural materials. Furthermore, the results of this study make it amply clear that the understanding of electronic structure and inter-atomic bonding characteristics is essential for the interpretation of experimental spectroscopic data as well as for the development of realistic
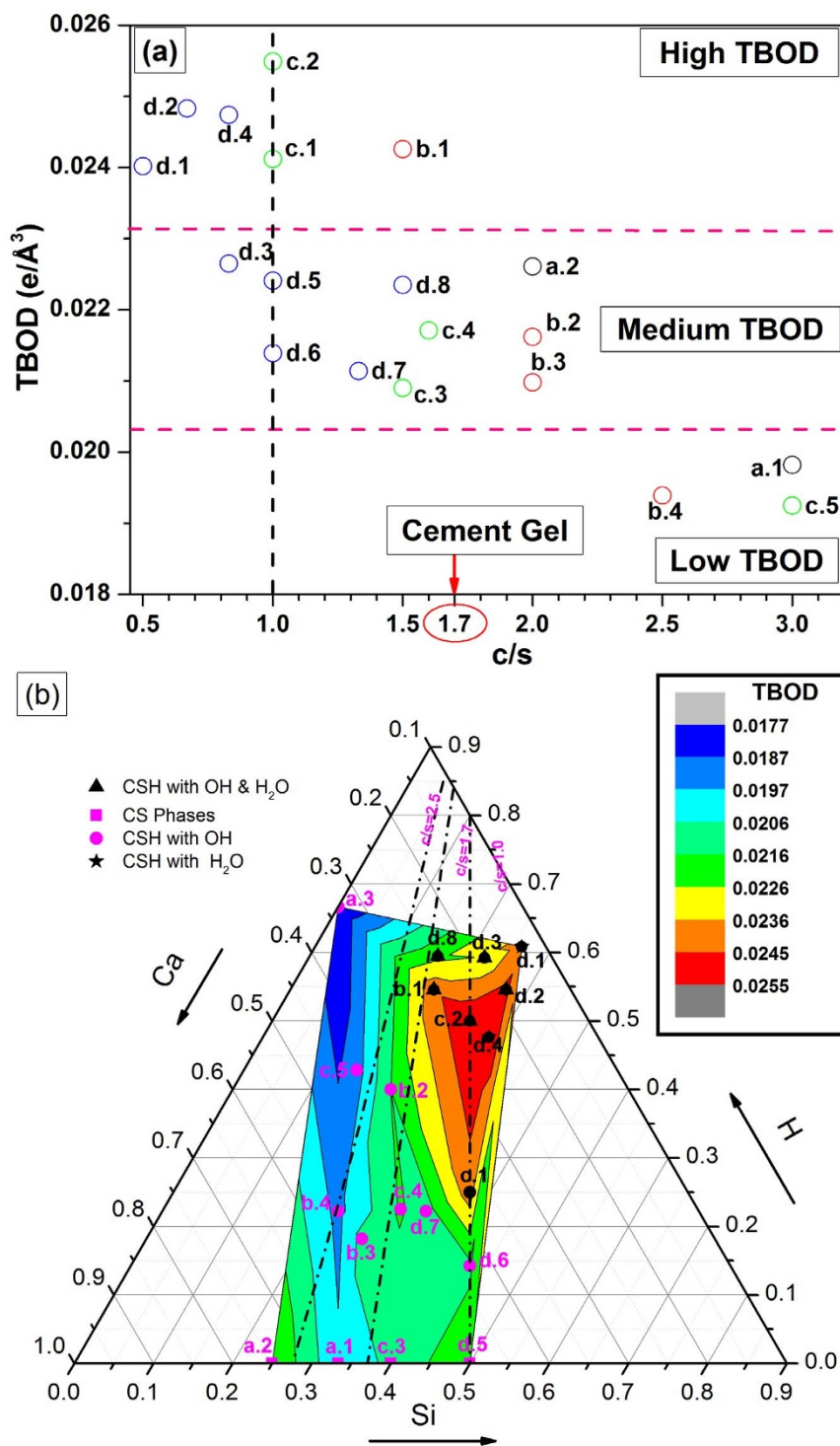
Figure 3 | (a) Total bond order density vs. C/S ratio in 19 crystals. (Portlandite (a.3) was excluded since it has no Si atoms.); (b) TBOD distribution map vs. the composition of Ca:Si:H. The color bar labels the values for the TBOD. The dot-dash lines indicate specific C/S ratios.

structural models of disordered cement hydrates. The approach used in this study has application to a broad class of complex material systems that incorporate covalent, ionic and hydrogen bonds, such as the apatite mineral class relevant to biological systems.

Methods

Crystal structural relaxation. For structural relaxation of the CSH crystals, we used the Vienna *ab initio* simulation package (VASP)[44,45]. The technical details are briefly outlined as follows: (1) the PAW-PBE potentials[46,47] with the generalized gradient approximation (GGA) is used. (2) The electronic convergence criterion is set at

10^{-6} eV. (3) The force convergence criterion is set at 10^{-5} eV/Å for ionic relaxation. (4) A high energy cutoff of 500 eV is adopted and (5) A sufficiently large number of *k*-point-meshes ranging from 2 to 85 k-points are used depending on the actual crystal structure and size.

Bond order density. For electronic structure and bonding analysis, we used the orthogonalized linear combination of atomic orbitals (OLCAO) method[23,48] based on the VASP-relaxed crystal structures. The bond order values for each crystal are calculated using Mullikan population analysis[49]. A more detailed description of the BO calculation is included in the SI. The TBOD is obtained as the cumulative total BO from all unique bond pairs divided by the cell volume. The percentage contribution of BO does not include the covenant O-H bonds of the water

molecules since they do not directly contribute to the internal cohesion of the crystal.

1. Richardson, I. G. The calcium silicate hydrates. *Cement Concrete Res* **38**, 137–158 (2008).
2. Bernal, J. D. The structures of cement hydration compounds. Paper presented at Proc. 3rd Int. Symp. Chem. Cem., London: Cement and Concrete Association. pp. 216–236 (1952).
3. Taylor, H. & Howison, J. Relationships between calcium silicates and clay minerals. *Clay Minerals Bull* **3**, 98–111 (1956).
4. Glasser, F. P., Lachowski, E. E. & Macphee, D. E. Compositional Model for Calcium Silicate Hydrate (C-S-H) Gels, Their Solubilities, and Free Energies of Formation. *J Am Ceram Soc* **70**, 481–485 (1987).
5. Taylor, H. F. W. & Roy, D. M. Structure and Composition of Hydrates at *7th International Congress on the Chemistry of Cement: Principal Reports,* Paris. Editions Septima, PII 2/1–13 (1980).
6. Dolado, J. S. & Van Breugel, K. Recent advances in modeling for cementitious materials. *Cement Concrete Res* **41**, 711–726 (2011).
7. Cong, X. & Kirkpatrick, R. J. ^{29}Si MAS NMR study of the structure of calcium silicate hydrate. *Adv Cem Based Mater* **3**, 144–156 (1996).
8. Pellenq, R. J.-M. *et al.* A realistic molecular model of cement hydrates. *P Natl Acad Sci USA* **106**, 16102–16107; DOI:10.1073/pnas.0902180106 (2009).
9. Taylor, H. F. W. Proposed Structure for Calcium Silicate Hydrate Gel. *J Am Ceram Soc* **69**, 464–467 (1986).
10. Taylor, H. F. W. Tobermorite, jennite, and cement gel. *Zeitschrift für Kristallographie* **202**, 41 (1992).
11. Pellenq, R.-M., Caillol, J. & Delville, A. Electrostatic attraction between two charged surfaces: a (N, V, T) Monte Carlo simulation. *J Phys Chem B* **101**, 8584–8594 (1997).
12. Dolado, J. S., Griebel, M. & Hamaekers, J. A molecular dynamic study of cementitious calcium silicate hydrate (C–S–H) gels. *J Am Ceram Soc* **90**, 3938–3942 (2007).
13. Richardson, I. G. The nature of C-S-H in hardened cements. *Cement Concrete Res* **29**, 1131–1147 (1999).
14. Dharmawardhana, C. C., Misra, A., Aryal, S., Rulis, P. & Ching, W. Y. Role of interatomic bonding in the mechanical anisotropy and interlayer cohesion of CSH crystals. *Cement Concrete Res* **52**, 123–130 (2013).
15. Strunz, H. *Mineralogische Tabellen.* (Akad. Verl.-Ges. Geest u. Portig, 1982).
16. Jennings, H. M. A model for the microstructure of calcium silicate hydrate in cement paste. *Cement Concrete Res* **30**, 101–116 (2000).
17. Tennis, P. D. & Jennings, H. M. A model for two types of calcium silicate hydrate in the microstructure of Portland cement pastes. *Cement Concrete Res* **30**, 855–863 (2000).
18. Cong, X. & James Kirkpatrick, R. ^{17}O and ^{29}Si MAS NMR study of β–C2S hydration and the structure of calcium-silicate hydrates. *Cement Concrete Res* **23**, 1065–1077 (1993).
19. Thomas, S., Meise-Gresch, K., Müller-Warmuth, W. & Odler, I. MAS NMR Studies of Partially Carbonated Portland Cement and Tricalcium Silicate Pastes. *J Am Ceram Soc* **76**, 1998–2004 (1993).
20. Garbev, K., Black, L., Beuchle, G. & Stemmermann, P. Inorganic polymers in cement based materials. *Wasser-und Geotechnologie* **1**, 19–31 (2002).
21. De la Torre, Á. G., De Vera, R. N., Cuberos, A. J. M. & Aranda, M. A. G. Crystal structure of low magnesium-content alite: Application to Rietveld quantitative phase analysis. *Cement Concrete Res* **38**, 1261–1269 (2008).
22. Haslingerová, I. Estimation of bond energies from mulliken overlap populations. *Czech J Phys* **27**, 1389–1393 (1977).
23. Ching, W.-Y. & Rulis, P. *Electronic Structure Methods for Complex Materials: The orthogonalized linear combination of atomic orbitals* 24 (Oxford University Press, USA, 2012).
24. Rastsvetaeva, R. K., Chukanov, N. V. & Zadov, A. E. Refined structure of afwillite from the northern Baikal region. *Crystallogr. Rep.* **54**, 418–422 (2009).
25. Richardson, I., Skibsted, J., Black, L. & Kirkpatrick, R. J. Characterisation of cement hydrate phases by TEM, NMR and Raman spectroscopy. *Adv Cem Res* **22**, 233–248 (2010).
26. Doyle, S. G. *Construction and Building: Design, Materials, and Techniques.* (Nova Science Publishers, Incorporated, 2010).
27. Malik, K. M. A. & Jeffery, J. W. A re-investigation of the structure of afwillite. *Acta Crystallogr B* **32**, 475–480 (1976).
28. Kim, J., Schmitt, U. W., Gruetzmacher, J. A., Voth, G. A. & Scherer, N. E. The vibrational spectrum of the hydrated proton: Comparison of experiment, simulation, and normal mode analysis. *J Chem Phys* **116**, 737–746 (2002).
29. Agrell, S. O. & Gay, P. Kilchoanite, a polymorph of rankinite. *Nature* **189**, 743–743 (1961).
30. Roy, D. M., Gard, J. A., Nicol, A. W. & Taylor, H. F. W. New Data for the Calcium Silicate, 'Phase Z'. *Nature* **188**, 1187–1188 (1960).
31. Zhesheng, M., Nicheng, S., Guodong, M. & Libing, L. Crystal structure refinement of suolunite and its significance to the cement techniques. *Chin. Sci. Bull.* **44**, 2125–2130 (1999).
32. Ito, T.-i., Sadanaga, R., Takéuchi, Y. & Tokonami, M. The existence of partial mirrors in wollastonite. *P Jpn Acad Sci* **45**, 913–918 (1969).
33. Velez, K., Maximilien, S., Damidot, D., Fantozzi, G. & Sorrentino, F. Determination by nanoindentation of elastic modulus and hardness of pure constituents of Portland cement clinker. *Cement Concrete Res* **31**, 555–561 (2001).
34. Ulm, F., Bazant, Z. & Wittman, F. *Creep, Shrinkage, and Durability Mechanics of Concrete and Other Quasi-Brittle Materials.* [197–203] (Elsevier, Amsterdam, 2001).
35. Constantinides, G. & Ulm, F.-J. The nanogranular nature of C–S–H. *J Mech Phys Solids* **55**, 64–90 (2007).
36. Beaudoin, J. J. Comparison of mechanical properties of compacted calcium hydroxide and portland cement paste systems. *Cement Concrete Res* **13**, 319–324 (1983).
37. Wittmann, F. H. Estimation of the modulus of elasticity of calcium hydroxide. *Cement Concrete Res* **16**, 971–972 (1986).
38. Monteiro, P. J. M. & Chang, C. T. The elastic moduli of calcium hydroxide. *Cement Concrete Res* **25**, 1605–1995 (1995).
39. Manzano, H., Dolado, J. S. & Ayuela, A. Elastic properties of the main species present in Portland cement pastes. *Acta Mater* **57**, 1666–1674 (2009).
40. Oh, J. E., Clark, S. M., Wenk, H.-R. & Monteiro, P. J. M. Experimental determination of bulk modulus of 14Å tobermorite using high pressure synchrotron X-ray diffraction. *Cement Concrete Res* **42**, 397–403 (2012).
41. Cong, X. & Kirkpatrick, R. J. ^{29}Si and ^{17}O NMR investigation of the structure of some crystalline calcium silicate hydrates. *Adv Cem Based Mater* **3**, 133–143 (1996).
42. Manzano, H. *Atomistic Simulation Studies of the Cement Paste Components,* PhD thesis, University of the Basque Country UPV/EHU, (15th July 2009).
43. Misra, A. & Ching, W. Theoretical nonlinear response of complex single crystal under multi-axial tensile loading. *Sci. Rep.* **3**, 1488; DOI:10.1038/srep01488(2013).
44. Kresse, G. & Hafner, J. Ab initio molecular dynamics for liquid metals. *Phys Rev B* **47**, 558–561 (1993).
45. Kresse, G. & Furthmüller, J. Efficiency of ab-initio total energy calculations for metals and semiconductors using a plane-wave basis set. *Comp Mater Sci* **6**, 15–50 (1996).
46. Blöchl, P. E. Projector augmented-wave method. *Phys Rev B* **50**, 17953–17979 (1994).
47. Perdew, J. P. Accurate Density Functional for the Energy: Real-Space Cutoff of the Gradient Expansion for the Exchange Hole. *Phys Rev Lett* **55**, 1665–1668 (1985).
48. Ching, W. Y. Theoretical Studies of the Electronic Properties of Ceramic Materials. *J Am Ceram Soc* **73**, 3135–3160 (1990).
49. Mulliken, R. S. Electronic Population Analysis on LCAO[Single Bond]MO Molecular Wave Functions. I. *J Chem Phys* **23**, 1833–1840 (1955).

Acknowledgments

Author contributions

W.Y.C. and A.M. designed the research; C.C.D. and W.Y.C. performed the calculations; all authors analyzed the data; all authors contributed to the discussion and wrote the paper.

Additional information

Supplementary information accompanies this paper at http://www.nature.com/scientificreports

Competing financial interests: The authors declare no competing financial interests.

How to cite this article: Dharmawardhana, C.C., Misra, A. & Ching, W.Y. Quantum Mechanical Metric for Internal Cohesion in Cement Crystals. *Sci. Rep.* **4**, 7332; DOI:10.1038/srep07332 (2014).